Morphological Changes during Secondary Crystallization and Subsequent Melting in Poly(ether ether ketone) as Studied by Real Time Small Angle X-ray Scattering

Ravi Verma,*,†,‡,§,⊥ Herve Marand,†,‡ and Benjamin Hsiao§

Materials Science and Engineering Department and Chemistry Department, NSF Science and Technology Center for High Performance Polymeric Adhesives and Composites, Virginia Polytechnic Institute & State University, Blacksburg Virginia 24061, and DuPont Central Research and Development, Experimental Station, Wilmington Delaware 19880

Received November 21, 1995; Revised Manuscript Received May 10, 1996[⊗]

ABSTRACT: In this paper, we present results of morphological studies during long time melt crystallization and subsequent melting in poly(aryl ether ether ketone) (PEEK). Morphological changes were monitored via small angle X-ray scattering (SAXS). SAXS data were analyzed via a combination of the correlation and interface distribution functions. Our analysis indicates the following: (1) The semicrystalline morphology is best described by a three-phase, dual lamellar stack model. Stacks of a finite number of lamellae and interlamellar amorphous layers are separated from each other by interstack regions of amorphous material (liquid pockets). (2) Secondary crystallization occurs via the formation of secondary lamellar stacks within the liquid pockets. Secondary lamellae are thinner than primary lamellae (70 Å vs 120 Å), and the amorphous layer thicknesses are about 47 Å in both stacks. (3) The low endotherm observed during a heating scan is associated with the melting of the secondary lamellae. (4) At room temperature, the semicrystalline PEEK material is in a state of dilational stress (negative hydrostatic pressure) which may originate from the secondary crystallization process in constrained liquid pockets.

Introduction

Poly(aryl ether ether ketone) (PEEK) is a semiflexible semicrystalline polymer which exhibits dual endothermic behavior during heating.[1−4] During heating in a differential scanning calorimeter (DSC), a low endotherm is observed at about 5−25 °C above the crystallization temperature, in addition to the high endotherm observed at about 340 °C.[4] This behavior is generally referred to as dual endothermic melting behavior, and since it has also been reported for other semicrystalline polymers,[5−9] it is now believed to be general to the class of semiflexible semicrystalline polymers which do not exhibit crystalline α_c relaxation.[10] There are two notable features of the low endotherm: (1) It increases in magnitude and shifts to higher temperatures with increasing crystallization time.[9,11] (2) The rate of increase of the magnitude of the low endotherm increases with temperature,[12−14] but the shift rate of the low endotherm to higher temperatures is independent of annealing temperature.[11,13,15]

Various morphological models have been proposed for the low endotherm.[16] These can be categorized as the dual lamellar population models[17,18] and the melting recrystallization model.[1−3,19,20] Let us first consider the dual lamellar population model, which was originally proposed by Bassett et al.[17] and by Cebe and Hong[18] and was subsequently extended by other authors.[21−25] According to this model, there exists a bimodal distribution of lamellar thicknesses within the semicrystalline polymer, with melting of thinnner and thicker lamellae associated with the low and high endotherms, respectively. The two variants of this model are the dual lamellar stack model[25] (with the thick and thin lamellae in *separate* stacks) and the lamellar insertion model[21−24] (with the thin lamellae inserted between thicker lamellae in the *same* stack). The lamellar stack model was based on the observation, made via transmission electron microscopy (TEM) techniques,[25] of two distinctly different types of lamellar stacks at room temperture. The primary argument in favor of lamellar insertion comes from the observation using time resolved small angle X-ray scattering (SAXS) techniques[21−24] that the long spacing and lamellar thickness decreases during the initial stage of crystallization. However, we have argued that the SAXS data is incompatible with the lamellar insertion model.[26] Our argument was based on the following observations: (1) During a heating scan, the average amorphous layer thickness decreases at temperatures corresponding to the low endotherm. Melting of thin secondary lamellae inserted between thicker primary lamellae would have increased the average amorphous layer thickness. (2) We noted that the observed decrease in the average lamellar thickness and long spacing during the initial stages of crystallization corresponds to the primary crystallization. These time scales are associated with to the development of the high endotherm.

The melting−recrystallization model was first proposed by Ikeda[27] and was subsequently supported by other authors for both poly(ethylene terephthalate) (PET)[1,28] and PEEK.[2,3,19,20,29,30] According to this model, the lamellae present initially melt and give rise to the low endotherm, but the melted material undergoes a continuous process of recrystallization into lamellae which melt at higher temperatures. Ultimately, melting dominates recrystallization, giving rise to the observed high endotherm. This model is based primarily on the observation that the magnitude and position of the low endotherm is heating rate dependent, but it does not account for various observations made by several authors. For example, it is now established that the high endotherm develops before the low endotherm.[4,11,17,26] Clearly, this last observation is not compatible with the assignment of the low endotherm to the melting of

† Materials Science and Engineering Department, Virginia Institute of Technology.
‡ Chemistry Department, Virginia Polytechnic Institute & State University.
§ DuPont Central Research and Development.
⊥ Present address: Chemical Engineering Department, California Institute of Technology, Pasadena, CA 91125.
⊗ Abstract published in *Advance ACS Abstracts,* October 15, 1996.

S0024-9297(95)01727-X CCC: $12.00

crystals formed during the primary crystallization stage. Here, we would like to mention that while we question the melting−recrystallization explanation for the low endotherm, we do not dispute the phenomenon of melting−recrystallization per se. Indeed, in a separate study,[31] we concluded that substantial melting−recrystallization occurs during heating of an initially amorphous PET sample. However, the corresponding DSC scan demonstrates only one endotherm.

For the reasons listed above, we are inclined to believe that the dual lamellar stack model is the appropriate explanation for the dual endothermic melting behavior. If the model is accurate, then the following observations are expected, but have not yet been made: (1) first, during long time annealing at any temperature, the development of the low endotherm should be accompanied by a decrease in average long spacing and lamellar thickness,[32] and (2) second, during a continuous heating scan, at temperatures corresponding to the low endotherm, there should be an increase in average long spacing and lamellar thickness that is brought about by melting of whole stacks of thin lamellae. While this observation has been made previously,[21,24,26] it is not clear whether the increase is brought about by melting from separate stacks or from within a stack.

Following the arguments presented in this section, we have monitored the evolution of the morphology during long time (up to 3 h) isothermal crystallization and subsequent melting in PEEK via SAXS. We have analyzed the SAXS data for detailed morphological information via a combination[33] of the correlation[34] and interface distribution functions.[35] Our analysis suggests the following: (1) The semicrystalline morphology is best described by a three-phase, dual lamellar stack model. These are the primary and secondary lamellar stacks, which are separated by interfibrillar regions of amorphous material (liquid pockets). Within a lamellar stack, the crystalline lamellae are separated by interlamellar amorphous layers. The SAXS data suggest that the two lamellar stacks have similar interlamellar amorphous layer thicknesses (about 47 Å), whereas primary lamellae are thicker than secondary lamellae (120 Å vs 70 Å). (2) During isothermal crystallization, the primary lamellar stacks form first. The rate of formation of the secondary lamellar stacks is linear with the logarithm of time, but increases with crystallization temperature. (3) During a heating scan, the secondary lamellae melt first, giving rise to the low endotherm. (4) There is a dilatational (negative) pressure within the semicrystalline sample. This negative pressure is responsible for the significant increase in the coefficient of thermal expansion of the noncrystalline fractions in the semicrystalline polymer, when compared to that of the equilibrium liquid at atmospheric pressure.

Experimental Section

PEEK samples were purchased from Atlantic Plastic Co. in Roanoke, VA, as amorphous sheets of grade 450 G and were used as received. SAXS data were collected using X-rays generated at a synchrotron source (Brookhaven National Laboratory Beamline X3A2; $\lambda = 1.542$ Å). The X-rays from the synchrotron source were focused with a silicon crystal monochromator and mirror and further collimated with three pinholes.[36] An evacuated flight path was used for the scattered X-rays, which was then monitored via a Braun linear position sensitive detector (pixel separation, 66.6 μm; 1024 pixels; sample to detector distance, 750 mm).

A dual chamber temperature jump unit was used for melt crystallization and subsequent melting. Detailed descriptions of this jump unit have been provided previously.[23,24] Briefly, for melt crystallization, the samples were melted at 385 °C for 4 min in one chamber and then pneumatically "jumped" to a second chamber maintained at the crystallization temperature. The estimated time for temperature equilibration at the crystallization temperature is about 30 s, although the initial 90% of the temperature change is spanned at about 300 °C/s. After thermal equilibration, the fluctuation in temperature was observed to be less than ±0.5 °C. The second temperature chamber was maintained at the crystallization temperature and was aligned in the path of the X-ray beam.

SAXS Data Analysis

Calculating the Correlation and Interface Distribution Functions. SAXS data were analyzed via a combination[33] of the correlation[34] and the interface distribution function[35,37] (see eqs 1−3). The correlation function (eq 1) is the Fourier transform of the Lorentz corrected SAXS profile.[34] The interface distribution function (eq 2) is the Fourier transform of the interference function (eq 3).[35,37]

$$\frac{\gamma_{1,r}}{Q} = \frac{\int_0^\infty (I - I_b) q^2 \cos(qr) e^{\sigma^2 q^2} dq}{\int_0^\infty (I - I_b) q^2 \, dq} \tag{1}$$

$$\frac{g_{1,r}}{Q} = \frac{\int_0^\infty G_q \cos(qr) e^{\sigma^2 q^2} dq}{\int_0^\infty (I - I_b) q^2 \, dq} \tag{2}$$

$$G_q = K - (I - I_b) q^4 e^{\sigma^2 q^2} \tag{3}$$

In eqs 1−3, K is the Porod law constant (discussed below), I_b is the liquid scattering profile (also discussed below), and q is the scattering vector ($q = [4\pi/\lambda]\sin\theta$, where 2θ is the scattering angle). Note that both the correlation function ($\gamma_{1,r}$) and the interface distribution function ($g_{1,r}$) are normalized with the scattering invariant (Q), which is related to the morphological variables by a relation summarized by eq 4.[21,38]

$$Q = \int_0^\infty (I - I_b) q^2 \, dq = \gamma_{1,0} = kx_{sph}x_{st} \frac{l_c}{l_c + l_a} \frac{l_a}{l_c + l_a} (\rho_c - \rho_{ila})^2 \tag{4}$$

In eq 4, k is a calibration constant, x_{sph} is the volume fraction of the spherulites in the material, x_{st} is the volume fraction of lamellar stacks within the spherulite, l_c and l_a are the average lamellar and amorphous layer thicknesses, and ρ_c and ρ_{ila} are the electron densities in the crystalline and interlamellar amorphous layers, respectively.

Since SAXS data are collected in a limited angular range (0.01 Å^{-1} < q < 0.23 Å^{-1}, in our case), it must necessarily be extrapolated to both high and low q values before Fourier transformation. The extrapolation to high q was performed with the aid of the Porod law given in eqs 5[39,40] and 6.[33]

$$\lim_{q\to\infty}[K - (I - I_b) q^4 e^{\sigma^2 q^2}] = 0 \tag{5}$$

$$\int_0^\infty [K - (I - I_b) q^4 e^{\sigma^2 q^2}] \, dq = 0 \tag{6}$$

In eqs 5 and 6, I_b is the contribution to total scattering arising from inhomogeneous density fluctuations and σ is related to the thickness of the crystal/amorphous interphase.[21] For eq 5, a Porod law region was defined

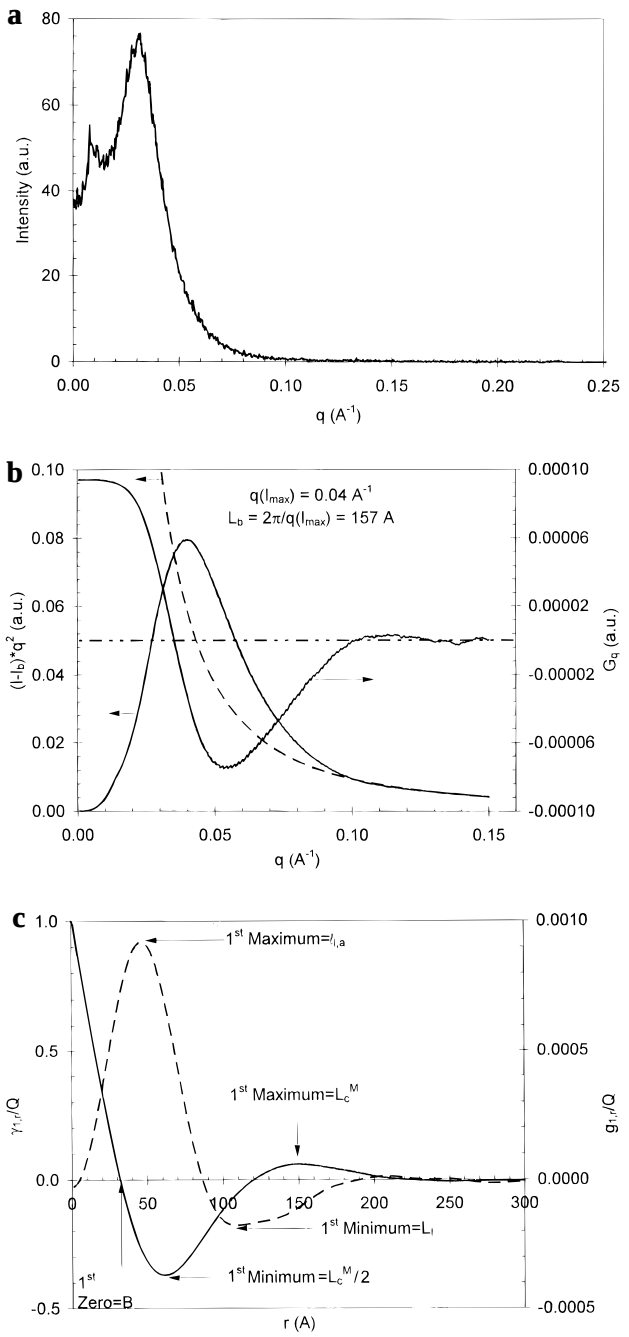

Figure 1. Illustration of the SAXS data analysis scheme. (a) A typical SAXS pattern. T_x, 312 °C; t_x, 2700 s. (b) The corresponding Lorentz-corrected plot and the interference function. (c) The normalized correlation function and the normalized interface distribution function.

as 0.11 Å^{-1} < q < 0.15 Å^{-1}. Other details of the Porod analysis are reported elsewhere.[33] Once the Porod constant K, the liquid scattering profile I_b, and the interface correction term σ have been estimated, the correlation and interface distribution functions can be easily calculated. This calculation is illustrated in Figure 1. Plot a in the figure depicts the raw scattering profile. Plot b depicts the corresponding Lorentz-corrected profile and the interference function, and plot c depicts the correlation and interface distribution functions.

Interpreting the Correlation and Interface Distribution Function. The correlation and interface distribution functions can be interpreted only with respect to a morphological model. We will begin by assuming the finite lamellar stack model. This model is comprised of stacks of crystalline lamellae separated by interlamellar amorphous layers, with adjacent lamellar stack separated by regions of interfibrillar amorphous material (liquid pockets). We will first extract the morphological parameters from the correlation function with respect to the finite lamellar stack model and then demonstrate that the lamellar thickness distribution is bimodal. This observation will enable the development of the dual lamellar stack model as the more appropriate morphological model.

The long spacing can be estimated as (1) the Bragg spacing corresponding to the peak in the Lorentz-corrected SAXS profile (L_B) (This estimate is illustrated in Figure 1b), (2) the position of the first maximum in the correlation function (L_c^M), (3) twice the position of the first minimum in the correlation function (L_c^m), and (4) the position of the first minimum in the interface distribution function (L_I). The estimates for L_c^M, L_c^m, and L_I are illustrated in Figure 1c.

The amorphous layer thickness can also be obtained via two different methods. First, the amorphous layer thickness can be estimated as the position of the first maximum in the interface distribution function ($l_{i,a}$). For the data depicted in Figure 1c, this estimate is about 47 Å. Second, a two-phase analysis of the correlation function yields estimates for average lamellar and amorphous layer thicknesses. Several methods have been outlined for this purpose.[41] The method that we have employed is summarized in eq 7.

$$\frac{B}{L_c^M} = x_{cl}(1 - x_{cl}) \tag{7a}$$

where x_{cl} is defined by

$$l_c = x_{cl}L_c^M \quad \text{and} \quad l_a = (1 - x_{cl})L_c^M \tag{7b}$$

In eq 7a, B is the position of the first intercept of the correlation function with the r axis. Note that eq 7 is quadratic in x_{cl} and can be solved to obtain two solutions for x_{cl}. The sum of these two solutions will equal 1, and only one of these solutions corresponds to the lamellar thickness. We will assume that the high value of x_{cl} is the appropriate solution. This is identical to assuming that the finite lamellar stack model is the appropriate morphological model. (If x_{cl} < 0.5, then the morphology would be adequately described by a two-phase model.) We will discuss this assumption in detail in a subsequent section. Based on our assignment for x_{cl}, the values for l_c and l_a can be easily obtained (104 and 46 Å, respectively, for the data depicted in Figure 1). Note that, within the experimental uncertainties, the estimate for the amorphous layer thickness from the correlation function (l_a = 46 Å) is identical to that obtained through the interface distribution function ($l_{I,a}$ = 47 Å). As we will demonstrate subsequently, these features are general to all the scattering profiles.

Let us now examine the different estimates of the long spacing. (1) First, we note that L_c^M does not correspond to L_c^m. Similar observations have been made previously.[26,42] According to the two-phase model,[41] the two estimates should be identical. For the correlation function depicted in Figure 1c, the two estimates differ substantially (150 Å vs 122 Å). The model calculations of Santa-Cruz et al.[42] and our own model calculations[33] suggest that $L_c^M > L_c^m$ when the thicker phase has a broader distribution of sizes than the thinner phase. In

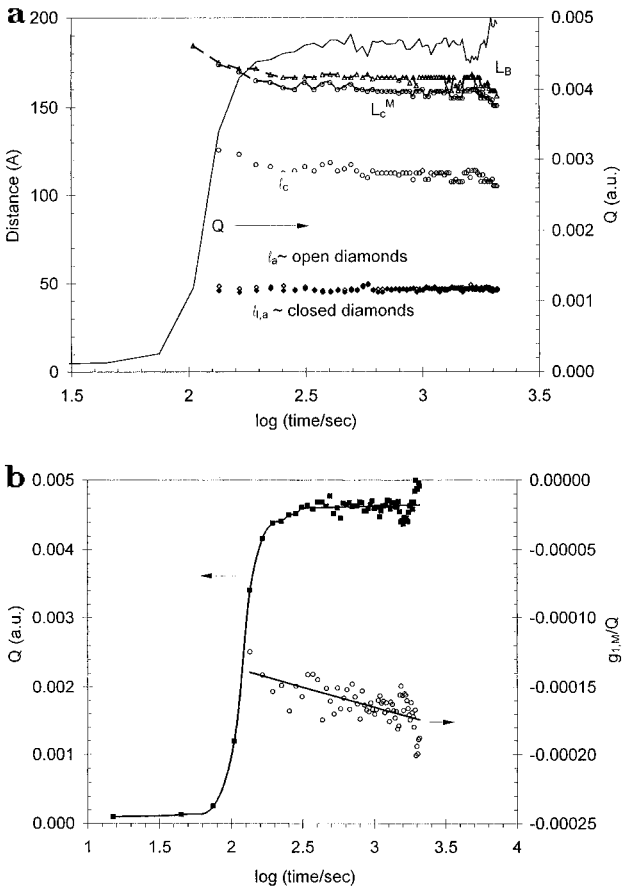

Figure 2. Morphological variables during isothermal melt crystallization and subsequent annealing at 300 °C. (a) The scattering invariant (Q), the different estimates for long spacing, the lamellar thickness (l_c) and amorphous layer thickness (l_a) obtained from the correlation function, and the amorphous layer thickness ($l_{I,a}$) as obtained from the interface distribution function. (b) The scattering invariant (Q) and the height of the first minimum in the normalized interface distribution function ($g_{1,M}/Q$).

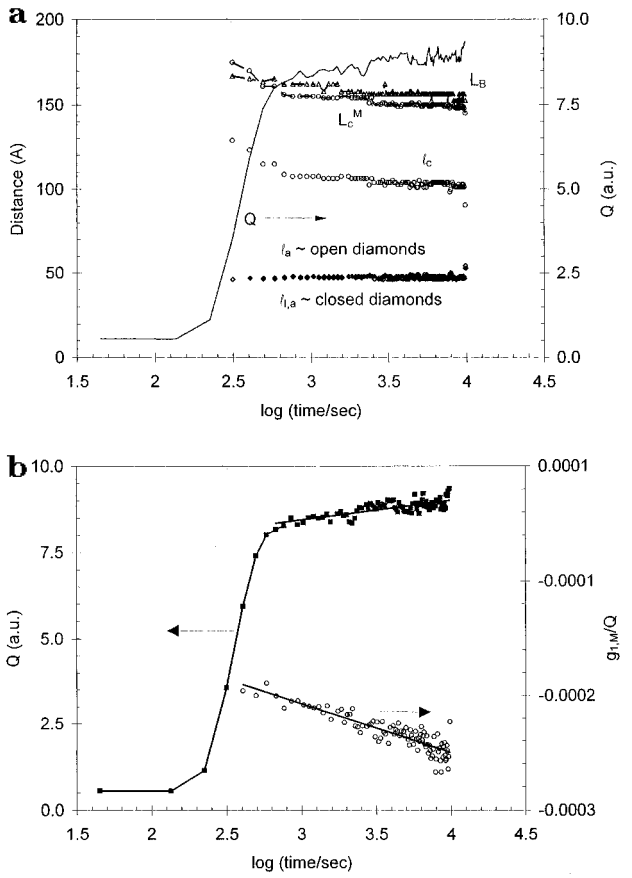

Figure 3. Morphological variables during isothermal melt crystallization and subsequent annealing at 312 °C. (a) The scattering invariant (Q), the different estimates for long spacing, the lamellar thickness (l_c) and amorphous layer thickness (l_a) obtained from the correlation function, and the amorphous layer thickness ($l_{I,a}$) as obtained from the interface distribution function. (b) The scattering invariant (Q) and the height of the first minimum in the normalized interface distribution function ($g_{1,M}/Q$).

our case, the thicker phase corresponds to the crystalline lamellae. Therefore, it can be concluded that the amorphous layer thickness is characterized by a narrower distribution than the lamellar thickness.

(2) Second, L_I is smaller than both L_c^m and L_c^M (109 Å vs 122 and 150 Å for the data depicted in Figure 1c). Similar observations have been reported previously for the case of PET.[42] Further, we observe that L_B is about 157 Å. In general, we observe that $L_B \geq L_c^M > L_c^m > L_I$. Santa-Cruz et al.[42] suggested that this inequality is caused by the presence of a distribution of long periods in the actual sample. Our model calculations[33] further suggested that the distribution of long periods is bimodal. Based on these observations, we formulated the dual lamellar stack model.[43] The dual lamellar stack model comprises primary and secondary lamellar stacks. Our analysis suggests that the primary lamellae are thicker than the secondary lamellae (120 Å vs 70 Å), while the amorphous layer thickness is similar in the two types of lamellar stacks.

In a previous publication,[33] we have outlined a procedure to deconvolute the interface distribution function with respect to the dual lamellar stack model. We have also demonstrated that the contribution from the secondary lamellar stacks to the total scattering is proportional to the height of the first minimum in the normalized interface distribution function. We will not employ the deconvolution procedure in this study because it is computationally intensive. Instead, we will use the height of the first minimum in the normalized interface distribution function [$g_{1,M}/Q$] as an estimate for the fraction of secondary lamellar stacks.

Results

The evolution of the morphology during crystallization at 300, 312, and 316 °C are depicted in Figures 2, 3 and 4, respectively. The total annealing time is 1 h at 300 °C (experiment summarized in Figure 2), and 3 h at 312 and 316 °C (Figures 3 and 4, respectively). The sample from the experiment of Figure 1 was cooled to room temperature (with the initial 150 °C being spanned at about 15 °C/min) and reheated at about 2.5 °C/min. Figure 5 summarizes the evolution of the morphological characteristics during reheating for this sample. Plot a in the figures includes traces for the scattering invariant Q, the different estimates of the long period, and the estimated lamellar and amorphous layer thicknesses. Plot b in the figures includes traces for the scattering invariant Q and the height of the first minimum in the normalized interface distribution function.

Several interesting features of the morphological variables during isothermal crystallization are readily apparent from Figures 2−4. (1) First, during primary crystallization (arbitrarily defined as the regime during which the invariant exhibits a sigmoidal increase with

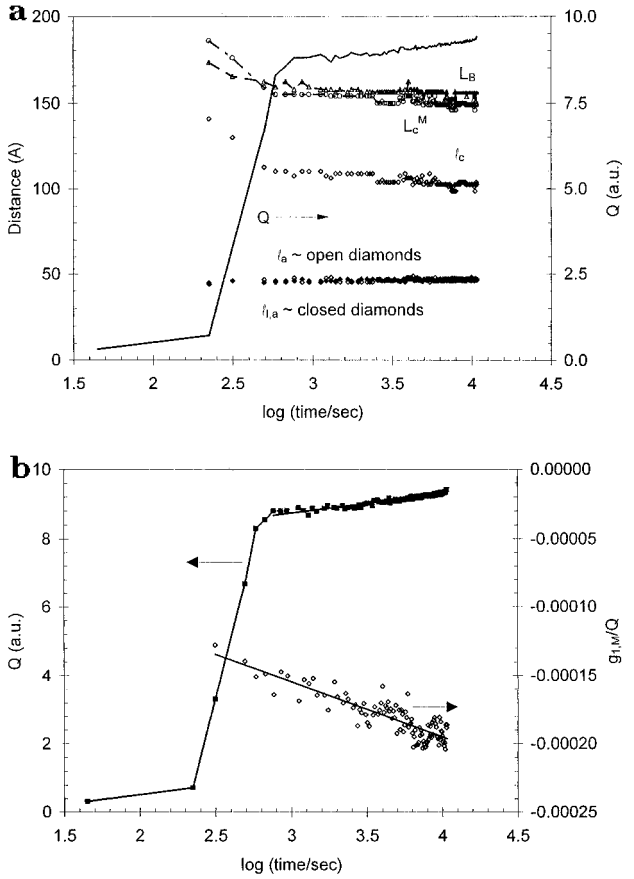

Figure 4. Morphological variables during isothermal melt crystallization and subsequent annealing at 316 °C. (a) The scattering invariant (Q), the different estimates for long spacing, the lamellar thickness (l_c) and amorphous layer thickness (l_a) obtained from the correlation function, and the amorphous layer thickness ($l_{l,a}$) as obtained from the interface distribution function. (b) The scattering invariant (Q) and the height of the first minimum in the normalized interface distribution function ($g_{1,M}/Q$).

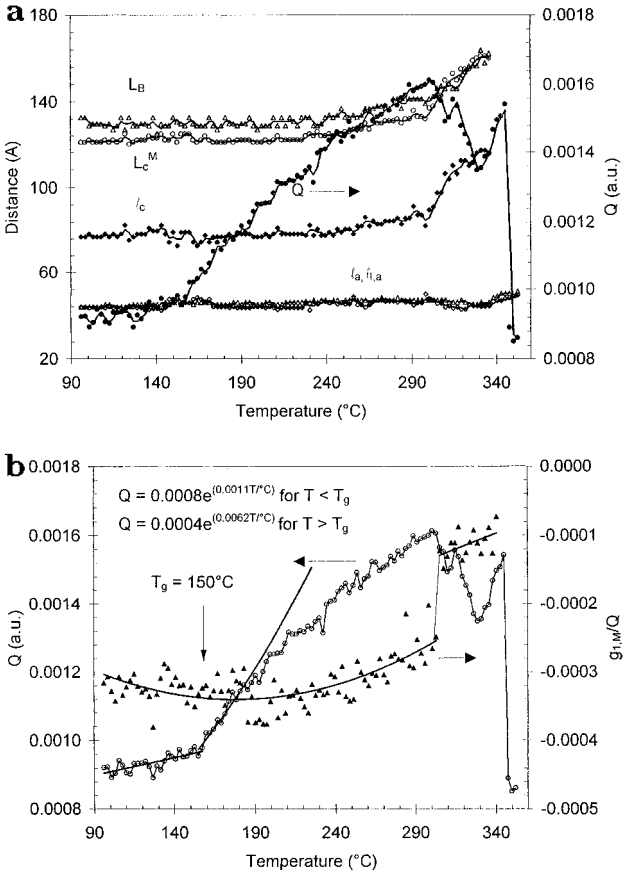

Figure 5. Morphological variables during heating at 2.5 °C/min of a PEEK sample isothermally crystallized at 300 °C for 1 h. (a) The scattering invariant (Q), the different estimates for long spacing, the lamellar thickness (l_c) and amorphous layer thickness (l_a) obtained from the correlation function, and the amorphous layer thickness ($l_{l,a}$) as obtained from the interface distribution function. (b) The scattering invariant (Q) and the height of the first minimum in the normalized interface distribution function ($g_{1,M}/Q$).

log time), the average long spacings (L_B and L_c^M) and the average lamellar thickness exhibit a systematic decrease (see plot a in Figures 2−4). Similar observations have been reported previously.[21,23] Calorimetric studies[4,12] indicate that this regime corresponds to the development of the high endotherm. This observation could be caused by insertion of subsidiary lamellae between two existing dominant lamellae, as suggested by some authors,[21,23,24] or by uncertainties in the estimate (the scattering power is fairly low, rendering the analysis difficult). (2) During secondary crystallization, the long spacing and average lamellar thickness exhibit a further decay that is approximately linear with log time (see plot a in Figures 2−4). Calorimetric studies[11−13] indicate that the low endotherm develops on this time scale. Therefore, our observations suggest that the development of the low endotherm is accompanied by a decrease in the average lamellar thickness and long spacings. (3) During secondary crystallization, the magnitude of the first minimum in the normalized interface distribution function increases linearly with log time (see plot b in Figures 2−4). On the basis of this observation, it can be concluded that the amount of secondary lamellar stacks increases linearly with log time during secondary crystallization.

Several interesting morphological changes are apparent during melting of the sample annealed at 300 °C for 1 h (see Figure 5). (1) The scattering invariant exhibits a change in slope at about 150 °C. This approximately corresponding to the glass transition temperature.[4] The change in slope implies a change in the thermal expansion coefficient of the interlamellar amorphous layer and/or the crystalline lamellae. Similar observations have been reported previously by several authors.[30,38] We will discuss this observation in a subsequent section. (2) The scattering invariant starts to decrease below the extrapolated straight line at about 200 °C (see Figure 5b). This decrease could be brought about by some premelting or by changes in the thermal expansion coefficients. (3) The invariant decreases sharply in a temperature range slightly above 300 °C, which approximately corresponds to the location of the low endotherm.[4] This decrease in the scattering invariant is accompanied by an apparent discontinuity in $g_{1,M}/Q$ (Figure 5b). (4) The long spacing increases dramatically in this same temperature range just above 300 °C. Both L_B and L_c^M increase to about 161 Å, which approximately corresponds to the long period estimated at the end of primary crystallization in Figure 2a. This observation suggests that the primary lamellar stacks have a long spacing of about 160 Å. The average lamellar thickness also increases during this temperature interval. On the basis of these observations and the observations discussed in the previous paragraph, one is led to conclude that the low endotherm is

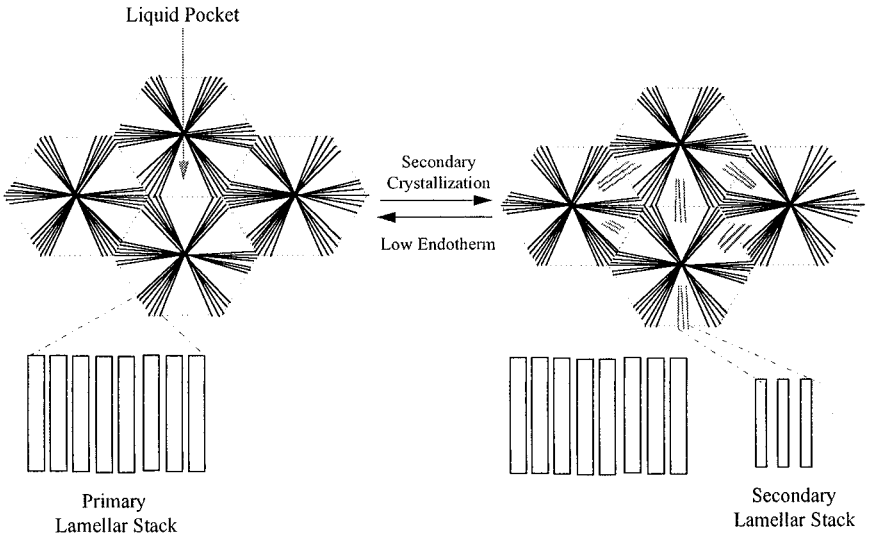

Figure 6. Model for the morphological changes that occur during secondary crystallization and subsequent melting. Note that the figure is not drawn to scale.

associated with the melting of lamellar stacks which formed during secondary crystallization.

Discussion

Morphological Changes during Secondary Crystallization and Melting. Primary crystallization results in the formation of spherulites comprised of primary lamellar stacks. These primary stacks are themselves comprised of about 5−10 lamellae and are separated from each other by liquid pockets which have dimensions on the order of 1000 Å.[25,44] Secondary crystallization occurs in these liquid pockets (see Figure 6) via the formation of secondary lamellar stacks, which comprise thinner lamellae than the primary lamellar stacks. Formation of secondary lamellae in the closed liquid pockets results in a decrease in the density of the remaining amorphous material in the liquid pockets. This, in turn, results in a negative pressure that is exterted on the lamellar crystals and, therefore, in a depression of the equilibrium melting temperature. During heating, the thinner secondary lamellae melt first, giving rise to the low endotherm. The position of the low endotherm will depend upon the magnitude of the negative pressure (which will determine the equilibrium melting temperature) and the lamellar thickness. Melting of the low endotherm will relieve the negative pressure in the liquid pockets, and therefore, the melting behavior of the primary lamellae will not be affected by the presence of secondary lamellae. Melting of the primary lamellae results in the high endotherm. Some speculative arguments on the underlying physical processes that causes crystallization to occur in the form of primary and secondary lamellar stacks have been presented earlier.[10,45] More detailed arguments will be presented in a subsequent publication.[46]

The Glass Transition and the Thermal Expansion Coefficient. Let us now revisit the issue of the glass transition. Cheng et al.[4] used calorimetric techniques to evaluate the fraction of the mobile amorphous segments and the degree of crystallinity for PEEK crystallized at various temperatures. They concluded that under most crystallization conditions (T_x < 300 °C, where T_x is the crystallization temperature), a fraction of the amorphous material does not contribute to the calorimetrically observed glass transition. They labeled this fraction as the rigid amorphous fraction (RAF). Experimental evidence supporting the existence of the RAF was provided by the dielectric spectroscopy work of Huo and Cebe[47] and that of Kalika and Krishnaswamy.[48] These authors further suggested that the RAF existed, even for T_x > 300 °C. According to Sauer and Hsiao,[49] this fraction corresponds to the interlamellar amorphous region. If that were the case, then the interlamellar amorphous fraction should behave like a glass, at least in a limited temperature range just above the T_g of amorphous PEEK. However, as depicted in Figure 5, the scattering invariant demonstrates a change in slope at about 150 °C. Similar observations have been reported by other authors.[30,38] An examination of Equation 4 suggests that this observation is consistent with an interlamellar amorphous fraction that relaxes at approximately 150 °C. Therefore, let us examine this observation in more detail. From eq 4, we have

Table 1. Thermal Expansion Coefficient ($\times 10^{-6}$ °C^{-1}) of the Individual Phases in the Semicrystalline Sample

	$T < T_g$	$T > T_g$
α_c	147[a]	250[a]
α_{ila}	282	777
$\alpha_{amorphous}$	175[b]	550[b]

[a] As quoted in ref 30. [b] From ref 51.

$$\frac{1}{Q}\frac{dQ}{dT} = 2\frac{\left(\frac{d\rho_c}{dT} - \frac{d\rho_{ila}}{dT}\right)}{(\rho_c - \rho_{ila})} = 2\frac{(\rho_{ila}\alpha_{ila} - \rho_c\alpha_c)}{(\rho_c - \rho_{ila})} \quad (8)$$

In eq 8, α_c and α_{ila} are the volume thermal expansion coefficients for the crystalline and the interlamellar amorphous fractions. Jonas et al.[30] have determined the thermal expansion coefficients of the crystalline phase (α_c) (see Table 1). Therefore, eq 8 can be used to estimate α_{ila}, which can then be compared with the volume thermal expansion coefficient of the unconstrained amorphous phase ($\alpha_{amorphous}$). In Table 1, we have listed $\alpha_{amorphous}$ both for $T \leq T_g$ (α_{glass}) and for $T > T_g$ (α_{liquid}).

Before we discuss α_{ila}, we will first consider $\alpha_{amorphous}$. We have previously determined[51] the thermal expansion coefficients of the amorphous phase in the glassy and liquid regions [α_{glass} and α_{liquid}, respectively]. Although

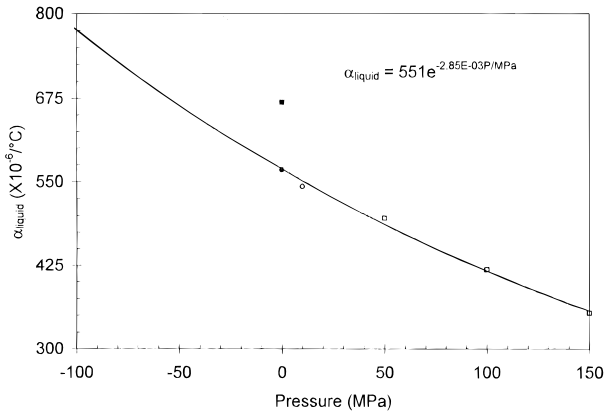

Figure 7. The variation of the thermal expansion coefficient with the applied external pressure. The open rectangles refer to the observed data of Zoller et al.[52] and the closed rectangle refers to the thermal expansion coefficient proposed by Zoller et al. The open circle refers to our[51] data, and the closed circle refers to our proposal for the thermal expansion coefficient.

our estimate for α_{liquid} is substantially lower than that reported by Zoller et al.[52] (550 vs 670 $\times$ 10^{-6} °C^{-1}), we believe it to be more accurate because (1) it is closer to the reported thermal expansion coefficient of other liquids.[53,54] For instance, the reported[55] value of α_{liquid} for isotactic polystyrene is 510 $\times$ 10^{-6} °C^{-1}. Furthermore, Choy and Leung[56] have determined the linear thermal expansion coefficient for the case of PEEK to be about 170 $\times$ 10^{-6} °C^{-1} at temperatures just above T_g.[57] We expect their technique to underestimate the overall thermal expansion coefficient (when estimated as $\alpha_{liquid} = 3\alpha_{liquid}^{linear}$) because some amount of fluid flow cannot be avoided in their measurement. However, we note that their estimate is in better agreement with our estimate than that of Zoller et al. (2) second, Zoller et al.[52] have measured the specific volumes at a series of pressures starting at 50 MPa. They have then estimated the specific volume at atmospheric pressure by isothermal extrapolations of the data. Given that the liquid state just above T_g is relatively inaccessible and that T_g shifts to higher temperatures with pressures, we believe that the isothermal extrapolation is erroneous for temperatures just above T_g. Specifically, isothermal extrapolation is performed via the Tait equation, which requires a parameter related to the bulk compressibility, κ. It is well-known that the bulk compressibility is a discontinuous function of temperature at T_g.[58] Furthermore, since the T_g shifts to higher temperatures with increasing pressures, the discontinuity in κ will also shift to higher temperatures with increasing pressures. This will undoubtedly affect the isothermal extrapolation significantly at temperatures just above T_g. On the other hand, our study[51] was performed at relatively lower pressures (10 MPa), and the observed thermal expansion coefficient at 10 MPa is about 543 $\times$ 10^{-6} °C^{-1}. The thermal expansion coefficient varies with the applied pressure as summarized below[59]

$$\alpha = \alpha_o e^{-\kappa P} \tag{9}$$

In eq 9, κ is the bulk compressibility and P is the external pressure applied to the sample. The variation in thermal expansion coefficient with pressure (see Figure 7) suggests that the thermal expansion coefficient at atmospheric pressure is about 550 $\times$ 10^{-6} °C^{-1} (filled circle on the plot, as reported by us[51]) and not 670 $\times$ 10^{-6} °C^{-1} (filled square on the plot, as reported by Zoller et al.[52]). Note that the value reported by Zoller et al. is far removed from the fitted curve.

Having introduced α_{liquid}, we can now turn our attention to the estimation of α_{ila}. We will do this by making an additional assumption that ρ_c and ρ_{ila} are 1.37 and 1.23 g/cm^3 at T_g[60] and applying these values to the data of Figure 5 via eq 8. This calculation yields estimates of 282 $\times$ 10^{-6} and 777 $\times$ 10^{-6} °C^{-1} below and above T_g, respectively. Note that the evaluation of α_{ila} has been performed in a temperature range 155 °C < T < 200 °C, which, according to Cheng et al., is well below the temperature at which the RAF starts changing. Similar results have been previously reported by Jonas et al.[30] These results are interesting for the following reasons: (1) If, as suggested by some authors,[20,21,29,30] the linear degree of crystallinity is 0.3, then the morphology can be adequately described by a two-phase model. If that were the case, then a simple mass balance between the crystalline and interlamellar amorphous fractions can be used to predict the overall thermal expansion coefficient. This estimate turns out to be 620 $\times$ 10^{-6} °C^{-1}. However, the overall thermal expansion coefficient[51] is only 400 $\times$ 10^{-6} °C^{-1}. Once again, this discrepancy cannot be ascribed to experimental errors and implies that a third phase *must* be invoked to account for the overall thermal expansion. (2) The estimated α_{ila} is substantially higher than $\alpha_{amorphous}$[51] (777 $\times$ 10^{-6} °C^{-1} vs 550 $\times$ 10^{-6} °C^{-1} above T_g, and 282 $\times$ 10^{-6} °C^{-1} vs 170 $\times$ 10^{-6} °C^{-1} below T_g[51,52]). This difference cannot be ascribed to experimental errors and indicates that the interlamellar amorphous layer *does not* behave like the unconstrained amorphous phase. An examination of Figure 7 suggests that the observed α_{ila} above T_g is consistent with a negative pressure of about 100 MPa. We note that, from the Clausius−Claypeyron equation, the melting temperature depression is about 0.483 °C/MPa.[52] Therefore, the data depicted in Figure 7 suggests that the depression in observed melting temperature brought about by the negative pressure is on the order of 48 °C. Finally, we note that this value corresponds, within experimental uncertainty, to the difference in the peak positions of the low and high endotherms (305 vs 340 °C).

The Linear Degree of Crystallinity. Inherent in our analysis of the SAXS data is the assumption that the linear degree of crystallinity is greater than 0.5. As already stated, this assumption is contrary to that made by a number of other authors.[20,21,29,30] However, it is not without precedence.[23,24,26,42] In this section, we would like to summarize the justifications for this specific assumption. (1) First, on thermodynamic grounds, the average lamellar thickness cannot decrease during a heating scan.[61] In some cases, we have observed[26] that this expectation is incompatible with x_{cl} < 0.5. On the other hand, the average lamellar thickness estimated with x_{cl} > 0.5 *never* decreases with increasing temperature, which is consistent with a gradual melting of thin lamellae. (2) Second, lower limits for the lamellar thickness can be obtained from a Scherrer line broadening analysis of the WAXD peaks. The estimate for lamellar thickness obtained from this analysis is always greater than the estimate obtained from the correlation function if x_{cl} < 0.5.[26,62,63] (3) The microscopy work of Lovinger et al.[64] suggests that the lamellar thickness is in the range of 100 Å for PEEK samples crystallized at high temperatures. Microscopy work of Liu and Geil[65] on PET (which is expected to be

similar to PEEK) indicates that the thickness of PET single crystals is about 70 Å for a wide range of polymerization temperatures, consistent with the high value for x_{cl}.[66] (4) The two possible solutions for x_{cl} (0.3 and 0.7) can be compared with the overall crystallinity of samples with similar thermal histories (estimated to be about 0.42 from DSC techniques[4] and about 0.48 from a Ruland analysis of the WAXD data[15]). The linear degree of crystallinity cannot be less than the overall crystallinity, and we note that the Ruland method yields absolute estimates for the crystallinity. (5) If $x_{cl} < 0.5$, then the linear degree of crystallinity would be about the same as the overall crystallinity. If that is the case, then thin lamellae separated by large interlamellar amorphous layers would uniformly fill the spherulite. No third phase would be present. As already demonstrated, this assumption leads to an overall thermal expansion coefficient of 560×10^{-6} °C^{-1}. However, the actual thermal expansion coefficient is much lower[51,56] (about 400×10^{-6} °C^{-1} for samples with similar thermal histories). This discrepancy can be explained only if a third phase (e.g. the amorphous fraction in liquid pockets) is invoked. (6) We feel that the estimate for lamellar thickness obtained with $x_{cl} < 0.5$ is physically unrealistic. For low crystallization temperatures, this estimate is in the range of 20−30 Å.[20,29,30] Note that this length scale corresponds to 2−3 crystallographic repeat units *and less than 1* chemical repeat unit. Clearly then, the appropriate solution for x_{cl} is the larger solution.

Conclusion

We have studied the morphological changes that occur during long time isothermal melt crystallization and subsequent melting in PEEK. Morphological changes were monitored via SAXS. SAXS data were analyzed via a combination of the correlation and the interface distribution function. From the correlation function, the average long spacing (L_c^M), the average lamellar thickness (l_c), and the average amorphous layer thickness (l_a) were estimated. From the interface distribution function, another estimate for the amorphous layer thickness ($l_{I,a}$) was obtained. Further, a comparison of the correlation function and the interface distribution function suggested that the semicrystalline morphology of PEEK is best described by a three-phase, dual lamellar stack model. From the heights of the first minimum in the interface distribution function, we were able to qualitatively estimate the relative amounts of the two lamellar stacks during both secondary crystallization and melting.

On the basis of our analysis of the SAXS data, we were able to make the following conclusions: (1) Primary lamellar stacks form first and are comprised of thicker crystalline lamellae compared to the secondary lamellar stacks. (2) The secondary lamellar stacks form as a function of log time during secondary crystallization. (3) During melting, the secondary lamellar stacks melt first, giving rise to the low endotherm. (4) There exists a negative pressure within the spherulite, and as a result, the thermal expansion coefficients of the noncrystalline fractions are higher than that of the unconstrained amorphous phase. This negative pressure is probably generated by the process of secondary crystallization in the constrained liquid pockets.

Acknowledgment. This study was made possible by generous financial support of several organizations. We gratefully acknowledge the Central Research and Development division of E. I. DuPont for their financial assistance and donation of beamtime. Additional support was provided by the NSF Science & Technology Center under DMR grant 912004. H.M. would like to thank the National Science Foundation for the Young Investigator award (DMR 9357512). Excellent technical assistance was provided by Mr. Joe McKeown of DuPont and by Mr. Paul Harney and Mr. Fengjie Ye of SUNY at Stony Brook. Finally, we would like to thank Dr. Greg McKenna of NIST, Gaithersburg, Md, for discussions on the effect of pressure on the thermal expansion behavior.

References and Notes

(1) Holdsworth, P. J.; Turner-Jones, A. *Polymer* **1971**, *12*, 195.
(2) Blundell, D. J.; & Osborn, B. N. *Polymer* **1983**, *24*, 953.
(3) Blundell, D. J. *Polymer* **1987**, 2248.
(4) Cheng, S. Z. D.; Cao, M. Y.; Wunderlich, B. *Macromolecules* **1986**, *19*, 1868.
(5) Lemstra, P. J.; Kooistra, T.; Challa, G. *J. Polym. Sci. A-2* **1972**, *10*, 823.
(6) Cheng, S. Z. D.; Pan, R.; Wunderlich, B. *Macromol. Chem.* **1988**, *189*, 2443.
(7) Bell, J. P.; Slade, P. E.; Dumbleton, J. H. *J. Polym. Sci. A-2*, **1968**, *6*, 1773.
(8) Cheng, S. Z. D.; Wu, Z. Q.; Wunderlich, B. *Macromolecules* **1987**, *20*, 2802.
(9) Roberts, R. C. *Polymer* **1969**, *117*.
(10) Marand, H.; Velikov, V.; Verma, R. K.; Cham, P. M.; Prabhu, V.; Dillard, D. *ACS Polym. Prepr.* **1995**, *36*(*1*), 263.
(11) Velikov, V.; Vivirito, J.; Marand, H. *ACS Polym. Prepr.* **1993**, *34* (*2*), 835.
(12) Velikov, V.; Marand, H., in preparation.
(13) Sholtz, P.; Prabhu, V.; Vivirito, J.; Marand, H., in preparation.
(14) Similar kinetics has also been reported for the phenomenon of lamellar thickening in poly(ethylene) and other flexible polymers. However, lamellar thickening is accompanied by an increase in long spacing, and the underlying physical processes are very different from the processes that accompany the development of the low endotherm in *semiflexible* semicrystalline polymers. Therefore, we have deliberately not cited the kinetics of lamellar thickening.
(15) Verma, R. K.; Hsiao, B. S.; Marand, H. in preparation.
(16) In the past, some of us proposed a model that was completely different from the models discussed in the text. We proposed that the low endotherm is the enthalpic recovery of a physically aged rigid amorphous fraction. We now acknowledge that we were in error. Therefore, we will not dwell on that explanation in the text.
(17) Bassett, D. C.; Olley, R. H.; Raheil, I. A. M. *Polymer* **1988**, *29*, 1745.
(18) Cebe, P.; Hong, S. D. *Polymer* **1986**, *27*, 1183.
(19) Lee, Y.; Porter, R. S. *Macromolecules* **1987**, *20*, 1336.
(20) Lee, Y.; Porter, R. S.; Lin, J. S. *Macromolecules* **1989**, *22*, 1756.
(21) Krüger, K.-N.; Zachmann, H. G. *Macromolecules* **1993**, *26*, 5202.
(22) Wang, J.; Alvarez, M.; Zhang, W.; Wu, Z.; Li, Y.; Chu, B. *Macromolecules* **1992**, *25*, 6943.
(23) Hsiao, B. S.; Gardner, K. H.; Wu, D. Q.; Chu, B. *Polymer* **1993**, *34* (*19*), 3986.
(24) Hsiao, B. S.; Gardner, K. H.; Wu, D. Q.; Chu, B. *Polymer* **1993**, *34* (*19*), 3996.
(25) Lattimer, M. P.; Hobbs, J. K.; Hill, M. J.; Barham, P. J. *Polymer* **1992**, *33*, 3971.
(26) Verma, R. K.; Kander, R. G.; Velikov, V.; Chu, B.; Hsiao, B. S.; Marand, H. *Polymer*, in press.
(27) Ikeda, M. *Chem. Abstr.* **1968**, *69*, 19666.
(28) Groeninckx, G.; Reynaers, H. *J. Polym. Sci. Polym. Phys. Ed.* **1980**, *18*, 1325.
(29) Jonas, A.; Legras, R. *Macromolecules* **1993**, *26*, 813.
(30) Jonas, A.; Russell, T. P., Yoon, D. *Macromolecules* **1995**, *28*, 8491.
(31) Verma, R. K.; Hsiao, B. S. *Macromolecules*, submitted.
(32) The reported decrease in long spacing and lamellar thickness during the initial stage of crystallization[21,22,23] can be ascribed to primary crystallization. As already pointed out,[26] this corresponds to the development of the high endotherm and not the low endotherm.

(33) Verma, R. K.; Biswas, A.; Hsiao, B. S.; Marand, H. *J. Appl. Cryst.* **1995**, submitted.
(34) Vonk, C. G.; Kortleve, G. *Colloid Polym. Sci.* **1967**, *220*, 19.
(35) Ruland, W. *Colloid Polym. Sci.* **1977**, *255*(*5*), 417.
(36) Chu, B.; Harney, P.; Li, Y.; Linhiu, K.; Ye, F.; Hsiao, B. *Rev. Sci. Instru.* **1994**, *65*(*3*), 597.
(37) Stribeck, N.; Ruland, W. *J. Appl. Cryst.* **1978**, *11*, 535.
(38) Gehrke, R.; Riekel, C.; Zachmann, H. G. *Polymer* **1989**, *30*, 1582.
(39) Koberstein, J. T.; Stein, R. S. *J. Polym. Sc., Polym. Phys. Ed.* **1983**, *21*, 2181.
(40) Ruland, W. *J. Appl. Cryst.* **1971**, *4*, 70.
(41) Strobl, G. R.; Schneider, M. *J. Polym. Sc., Polym. Phys. Ed.* **1980**, *18*, 1343.
(42) Santa-Cruz, C.; Stribeck, N.; Zachmann, H. G.; Calleja, B. J. *Macromolecules* **1991**, *24*, 5980.
(43) Verma, R. K.; Biswas, A.; Hsiao, B. S.; Marand, H. *J. Appl. Cryst.* **1995**, submitted.
(44) The dimensions for the liquid pockets are quoted for high crystallization temperatures only. For lower crystallization temperatures, we expect the average size of the liquid pockets to be lower.
(45) Hsiao, B. S.; Sauer, B. B.; Verma, R. K.; Zachmann, H. G.; Seifert, S.; Chu, B.; Harney, P. *Macromolecules* **1995**, *28*, 6931.
(46) Verma, R. K.; Marand, H., in preparation.
(47) Huo, P.; Cebe, P. *Macromolecules* **1992**, *25*, 902.
(48) Kalika, D. S.; Krishnaswamy, R. S. *Macromolecules* **1993**, *26*, 4252.
(49) Sauer, B. B.; Hsiao, B. S. *Polymer* **1994**, *36*, 2553.
(50) Strictly, eq 8 is valid only if x_c and x_{cl} are both constant. Therefore, eq 8 can be assumed to be valid only in a limited temperature range just above the glass transition.
(51) Verma, R. K.; Velikov, V.; Marand, H.; Sauer, B. B.; Dee, G. T., in preparation.
(52) Zoller, P.; Kehl, T.; Starkweather, H. W.; Jones, G. *J. Polym. Sci. Polym. Phys. Ed.* **1989**, *27*, 993.
(53) Kauzmann, W. *Chem. Rev.* **1948**, *43*, 219.
(54) Gibbs, J. H.; DiMarzio, E. A. *J. Chem. Phys.* **1958**, *28*, 373.
(55) Patnode, W.; Scheiber, W. *J. Am. Chem. Soc.* **1939**, *61*, 3449.
(56) Choy, C. L.; Leung, W. P. *J. Polym. Sci. Polym. Phys. Ed.* **1990**, *28*, 1965.
(57) The cited number was obtained from a visual estimate of Figure 3 in ref 56.
(58) See, for instance, Figure 3 in ref 52.
(59) In eq 9, we are treating the isothermal compressibility κ as independent of pressure. This is not strictly true (see, for instance, eq 6 in ref 52). Therefore, eq 9 is an approximation which we use only for illustration.
(60) The cited values are from refs 30, 51, and 52. ρ_c is read from Figure 2 of ref 30. For ρ_{ila}, we made the additional assumption that ρ_{ila} is similar to $\rho_{amorphous}$. $\rho_{amorphous}$ was then calculated from Table II of ref 52 and verified with our own work of ref 51. While the exact values may differ somewhat, the final calculations are, for the most part, unaffected by slight variations in the exact values.
(61) Although such an observation has been made for the case of polyethylene, it is not plausible for the case of PEEK because of the absence of a crystal α_c relaxation.
(62) Yoda, O. *Polym. Commun.* **1985**, *26*, 16.
(63) In general, the estimate is about 80 Å for PEEK crystallized at high temperatures.[26] In some cases, the estimate is lower. In ref 62, Yoda estimates the lamellar thickness and long spacing to be about 61 and 145 Å, respectively, for drawn PEEK crystallized at 300 °C. This implies that $x_{cl} = 0.42$, which is less than 0.7 but definitely greater than 0.3 (the two possible solutions for x_{cl} from the correlation function). However, we expect the average lamellar thickness to be altered somewhat in the drawn samples.
(64) Lovinger, A. J.; Hudson, S. D.; Davis, D. D. *Macromolecules* **1992**, *25*, 1752.
(65) Liu, J.; Geil, P. *Macromolecules*, **1996**, Preprint.
(66) Verma, R. K.; Sholtz, P.; Marand, H., in preparation.

MA951727O